processes

MDPI

Article

Automated Gas Influx Handling Model and Mechanisms During Deep High-Temperature and High-Pressure Well Drilling

Yanbin Zang [1,2], Wenping Zhang [1,2], Zhengming Xu [3,*], Jiayi Lu [3] and Zhilu Deng [3]

[1] State Key Laboratory of Shale Oil and Gas Enrichment Mechanisms and Efficient Development, Beijing 102206, China; zangyb.sripe@sinopec.com (Y.Z.); zhangwp.sripe@sinopec.com (W.Z.)
[2] SINOPEC Research Institute of Petroleum Engineering Co., Ltd., Beijing 102206, China
[3] School of Energy Resources, China University of Geosciences (Beijing), Beijing 100083, China; ljyi0704@163.com (J.L.); d163123321@163.com (Z.D.)
* Correspondence: xuzm@cugb.edu.cn

Abstract: The exploration and development of oil and gas resources in deep formations is a key strategic priority for national energy production. However, manual methods for handling gas kicks suffer from low operating accuracy and inefficiency during high-temperature and high-pressure deep well drilling. To address the need for real-time bottomhole pressure prediction and control, an efficient gas–liquid–solid computing model was developed based on the gas slip model and cuttings settling velocity model. By integrating this model with an automatic choke adjustment system, an automatic gas kick attenuation model for deep well drilling was established. Results show that, compared to the driller's and wait-and-weight methods, the automatic gas kick attenuation method significantly reduces peak choke pressure due to its larger frictional pressure drop and higher cuttings hydrostatic pressure. The automatic attenuation method not only leads to an average reduction of 28.42% in maximum choke/casing pressure but also accelerates gas removal, achieving gas kick attenuation ten times faster than the driller's method and seven times faster than the wait-and-weight method. The study also investigates the influence of gas solubility, well depth, gas influx volume, formation permeability, and drilling fluid volumetric flow rate on gas kick attenuation characteristics. The findings provide a solid foundation for improving the efficiency of gas kick management in deep well drilling operations.

Keywords: automatic gas kick attenuation; deep well; high temperature and high pressure; gas–liquid–solid flow

Citation: Zang, Y.; Zhang, W.; Xu, Z.; Lu, J.; Deng, Z. Automated Gas Influx Handling Model and Mechanisms During Deep High-Temperature and High-Pressure Well Drilling. *Processes* **2024**, *12*, 2558. https://doi.org/10.3390/pr12112558

Academic Editor: Francisco Vazquez

Received: 24 October 2024
Revised: 6 November 2024
Accepted: 13 November 2024
Published: 15 November 2024

1. Introduction

The exploration and development of oil and gas resources in high-temperature, high-pressure (HTHP) deep formations are critical for national energy strategies. These environments pose significant drilling challenges, characterized by narrow safety pressure windows and complex fluid dynamics, making accurate prediction of wellbore conditions difficult. If mishandled, gas influx can lead to catastrophic blowouts, as demonstrated by the 2010 Macondo disaster [1–4]. Therefore, real-time prediction and control of bottomhole pressure (BHP) are essential to prevent such incidents [5].

Accurate prediction of BHP after a gas influx in deep HTHP wells requires more advanced models than the gas–liquid two-phase flow models currently used. Cuttings in the annulus and convective heat transfer between the wellbore and the surrounding formation further complicate multiphase flow and heat transfer behavior, impacting the accuracy of BHP predictions. There is a notable gap in the research on gas–liquid–solid flow models for such environments, and improving the accuracy of BHP predictions after a gas influx remains a critical need.

Moreover, the long wellbore lengths in deep wells make gas influx handling with conventional methods, such as the driller's method (DM) and wait-and-weight method

(WWM), time-consuming and inefficient. Manual gas influx handling methods suffer from poor precision and low efficiency and require frequent pressure adjustments. This is particularly problematic in deep formations with narrow safety pressure windows, where improper gas influx handling can lead to secondary gas influx or formation fracturing, exacerbating drilling accidents [6,7]. Therefore, there is a pressing need for a safe and efficient automatic gas influx handling method for deep wells to improve operational efficiency and reduce non-productive time. By combining managed pressure drilling (MPD) with automatic gas influx handling, and using constant BHP as the control goal and choke pressure (choke opening) as the control target, gas influx in deep wells can be managed automatically and quickly, without the need to stop drilling or halt pump operations [8,9].

Many aspects of drilling have already been automated [10–12]. For example, Jansen and Steen [13] developed the Soft Torque Rotary System, which uses a feedback control system for motor current and speed to expand the operational range of stick–slip–free rotation by effectively lowering thresholds. The new generation of integrated AC top-drive systems has been installed on 60 drilling platforms globally and commercialized by industry suppliers [14]. Riet et al. [15] developed a fully automatic MPD system, which maintains constant BHP by controlling the choke valve opening and backpressure pump volumetric flow rate. This system can automatically calculate the backpressure required to maintain constant BHP, use computer control to generate the necessary backpressure through the choke manifold, and automatically circulate the invaded gas. It has been successfully implemented in several challenging deep-water operations. Kyllingstad and Nessjoen [16] developed a system using a proportional–integral (PI) controller to reduce cyclical fluctuations in drive torque and bit rotational speed. This system can also automatically determine stick–slip frequency, instantaneous bit speed, and stick–slip severity, and has been commercialized following successful field tests. Florence et al. [17] developed an automated drilling system optimized for multiple objectives, providing stable weight on bit and motor differential pressure to achieve a faster rate of penetration (ROP) and better wellbore quality. This system has been tested in several field applications, showing ROP and bit longevity improvements. Matheus and Naganathan [18] developed an automated well trajectory control system to maintain the well trajectory within the error range. Godhavn and Knudsen [19] created an automatic choke control system for MPD, which has been implemented in North Sea wells with narrow safety pressure windows. Dunlop et al. [20] developed a closed-loop system for real-time monitoring of drilling parameters and performance, continuously adjusting the weight on bit and rotational speed to automatically optimize ROP. This method has been tested at 13 different sites, demonstrating more than a 10% increase in ROP compared to non-automated operations. Cayeux et al. [21] developed an automated drilling fluid pump management system to minimize the risk of formation fracturing during pump startup and drilling fluid circulation. This system has been applied in the North Sea, along with other automation systems for drawworks and top drives to minimize sucker rod pumping effects. Many of these algorithms have been tested in the North Sea, and several have been commercialized [22]. Cayeux et al. [23] also analyzed surface and downhole measurement parameters required for drilling automation, identifying the key parameters and locations needed for physical models.

In the context of gas kick control, Carlsen et al. [24] developed an automatic coordination control system for drilling fluid pump volumetric flow rate and choke valve opening, using a multiphase transient flow model to evaluate dynamic shut-in procedures. Results showed that dynamic shut-in combined with automatic control significantly reduced well control time and overall operational risk compared to traditional methods. Gravdal et al. [25] proposed using downhole data from drill pipe telemetry to maintain pressure within expected ranges during gas influx control. This method estimates formation pore pressure in real-time based on gas influx and pressure recovery data, aiming to enhance MPD efficiency. Zhou et al. [26] developed a switching control system for annular pressure regulation, enabling automatic gas influx handling through choke valve and backpressure

pump management. Aarsnes et al. [27] created a first-order infinite system approximation and modified it for two-phase flow dynamics, using linear matrix inequalities for automatic gas influx control in MPD. Ma et al. [28] designed a transient gas influx simulator for water-based drilling fluids (WBDFs) and a PI controller for automatic choke valve adjustment to maintain constant BHP. This model addresses complex MPD well control issues, such as multi-point gas influx, sudden pump changes, and non-Newtonian fluids, and was later extended to oil-based drilling fluids (OBDFs) [29], accounting for gas dissolution and release effects. Sule et al. [30] developed a nonlinear model predictive controller for MPD systems, integrated with a two-phase flow model for automatic BHP control. Compared to a single-phase linear model, NMPC provided more accurate predictions of key well control parameters and responded faster to gas influx disturbances. Carlsen et al. [31] assessed various algorithms for automatic choke control, including proportional–integral–derivative (PID), the internal model, and model predictive controllers, optimizing their parameters. Hauge et al. [32] created an adaptive observer for multiphase flow systems to estimate unknown parameters and inflow/outflow rates, while also proposing a controller to suppress gas influx. Shishavan et al. [33] developed an integrated MPD controller to regulate drilling fluid pump volumetric flow rate, choke valve opening, drill string speed, and weight on bit, optimizing both ROP and BHP, thereby reducing costs, risks, and operator workload.

From the above literature, it is clear that existing automatic gas influx handling models primarily rely on single-phase or two-phase flow models, without accounting for the presence of cuttings in the annulus or convective heat transfer between the wellbore and formation [5,34,35]. This results in lower prediction accuracy of BHP, leading to frequent choke opening adjustments and further complicating multiphase flow and pressure transmission characteristics in the wellbore. Therefore, there is a need for further research to improve the accuracy and computational efficiency of BHP prediction during automatic gas influx handling in deep wells.

When managing gas influx, it is critical to control BHP within the range between formation pore pressure and fracture pressure to prevent secondary gas influx or formation fracturing. However, in deep wells, the long wellbore length results in significant time consumption when using traditional gas influx handling methods [36,37]. Furthermore, manual operations are often characterized by poor precision and low efficiency in managing gas influx. Therefore, developing an automated gas influx handling model for deep wells is essential to ensure safety and efficiency.

This study developed an efficient gas–liquid–solid flow calculation model based on the gas phase drift flow and cuttings settling velocity models to handle interphase slip, ensuring that the calculation efficiency meets the real-time requirements for predicting BHP. Additionally, an automated gas influx handling model was established by incorporating an automatic choke valve adjustment system based on PID control theory. The impact of controller parameters on automatic gas influx handling was analyzed, and comparisons were made between the DM and WWM. Finally, the effects of solubility, well depth, gas influx volume, formation permeability, and drilling fluid volumetric flow rate on automatic gas influx handling were analyzed.

2. Model Development

2.1. Establishment of Efficient Gas–Liquid–Solid Flow Calculation Model

Figure 1 presents the automated gas influx handling schematic in deep HTHP drilling. The key objective of automated gas influx handling is to maintain constant BHP in real-time while circulating the intruded gas out of the well. This is accomplished by adjusting the choke opening to generate the necessary throttling pressure. Real-time feedback of the BHP is essential for automatic choke adjustment, while the multiphase flow model's calculation time must be less than 1/300th of the simulated gas influx time to ensure a timely response.

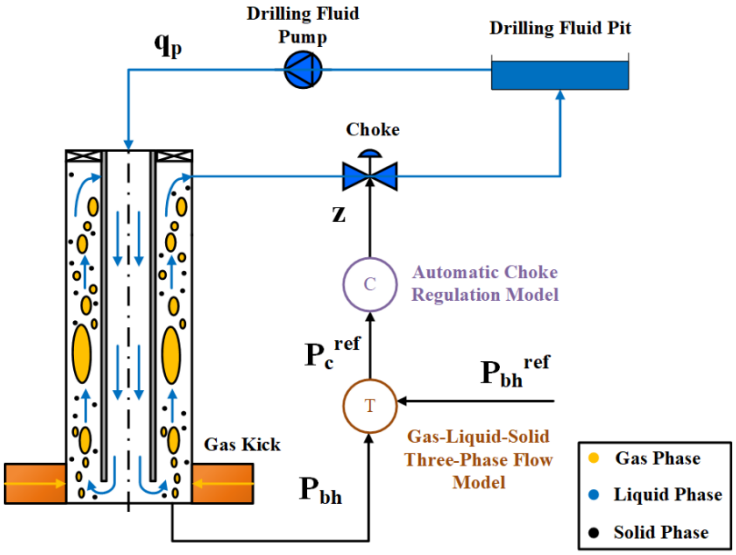

Figure 1. A schematic of the automatic gas kick attenuation during HTHP deep well drilling (Z is choke opening, P_c^{ref} is desired choke pressure, P_{bh} is actual bottomhole pressure, P_{bh}^{ref} is desired bottomhole pressure).

The momentum conservation equation is improved to enhance computational efficiency, based on the gas–liquid–solid flow mechanism model. Specifically, the momentum conservation equation for the gas–liquid–solid mixture is employed:

$$\frac{\partial}{\partial t}\left(\sum \rho_m \alpha_m V_m\right) + \frac{\partial}{\partial z}\left(P + \sum \rho_m \alpha_m V_m^2\right) + \sum \rho_m \alpha_m g \cos\theta + F_f = 0 \quad (1)$$

where ρ is density, in kg/m^3, α is volumetric fraction, V is velocity, in m/s, P is pressure, in Pa, g is gravitational acceleration, in m/s^2, θ is wellbore inclination, in °, F_f represents the frictional pressure drop of the annular mixture, in kg/m^2/s^2, and the subscript m denotes the gas, liquid, and solid phases (G, L, S).

The gas-phase drift flow model and cuttings settling velocity model are used to handle the slip velocity between the gas, liquid, and solid phases [38,39]. The slip between the gas and liquid phases can be expressed as follows [40]:

$$V_G = C_0^{G-L} V_M + V_{gr} \quad (2)$$

where V_G is gas velocity, in m/s, C_0^{G-L} represents the distribution parameter between the gas and liquid phases, V_M represents the velocity of the gas–liquid–solid mixture, in m/s, and V_{gr} represents the gas-phase slip velocity, in m/s. In this paper, the model established by Shi et al. [41] is used to calculate the distribution parameter and gas-phase slip velocity. This model has been widely applied [42–45]:

$$C_0^{G-L} = \frac{A}{1 + (A-1)\gamma^2} \quad (3)$$

$$V_{gr} = \frac{\left(1 - \alpha_G C_0^{G-L}\right) C_0^{G-L} K(\alpha_G) V_c}{\alpha_G C_0^{G-L} \sqrt{\rho_G / \rho_L} + 1 - \alpha_G C_0^{G-L}} (\cos\theta)^{0.5} (1 + \sin\theta)^2 \quad (4)$$

where A is a profile parameter for the low gas fraction in liquid, γ is a profile parameter reduction term, K is the critical Kutateladze number, and V_c is characteristic velocity, in m/s.

The slip velocity between the cuttings and the liquid phase can be expressed as follows:

$$V_S = C_0^{S-L} V_M^* - V_{sr} \quad (5)$$

where V_S represents the velocity of the cuttings, in m/s, C_0^{S-L} represents the distribution parameter between the cuttings and the liquid phase, V_M^* represents the velocity of the liquid–solid mixture in the annulus, in m/s, and V_{sr} represents the cuttings settling velocity, in m/s. In this paper, the distribution parameter between the cuttings and the liquid phase C_0^{S-L} is set to 1.05, and the cuttings settling velocity is calculated using the explicit prediction model:

$$V_{sr} = \left(\frac{4d_*}{3C_d}\right)^{\frac{1}{2}} \left(\frac{{\rho_L}^2}{\mu g(\rho_S - \rho_L)}\right)^{-\frac{1}{3}} \quad (6)$$

where d_* is dimensionless cuttings diameter, C_d is drag coefficient, and μ is fluid viscosity, in Pa·s.

The saturated solubility of invading gas in oil-based drilling fluid can be calculated using the following equation [46]:

$$R_s = 0.1781 \times SG_g \left[\frac{P \times 10^{0.0125API}}{18 \times 10^{0.00091(1.8T-459.67)}}\right]^{1.20482} \quad (7)$$

where R_s is the saturated gas solubility, in m^3/m^3, SG_g is the gas specific density, API is the API gravity of OBDF, and T is temperature, in K.

The gas influx simulation was conducted using Matlab R2016a software on an Intel i5-2400 CPU processor. The computational efficiency is defined as the ratio of the simulated gas influx time to the time consumed by the multiphase flow model calculations. The grid numbers were 100, 250, 500, 600, and 700, respectively. The computational efficiency of the gas–liquid–solid flow mechanism model and the efficient flow calculation model are shown in Table 1. Using the three-phase flow mechanism model, none of the five selected grid numbers can achieve the computational efficiency required for real-time prediction. However, using the efficient flow calculation model, real-time prediction requirements can be met when the grid number is 250 or fewer. Therefore, the grid number is set to 250 in all case analyses in this chapter. At 60,000 s, the BHP predicted by the gas–liquid–solid flow mechanism model and the efficient calculation model is 139.90 MPa and 139.54 MPa, respectively, with a BHP difference of 0.36 MPa. This means that compared to the three-phase flow mechanism model, the prediction accuracy of the efficient three-phase flow calculation model decreases by 0.26%.

Table 1. The computational efficiency for the gas–liquid-solid mechanistic model and the efficient computing model.

Grid Number	Gas–Liquid-Solid Mechanistic Model	Efficient Computing Model
100	149	1736
250	36	324
500	16	87
600	11	61
700	7	45

To validate the accuracy of the established gas–liquid–solid three-phase flow model, the model's predictions were compared with experimental results from the literature [47]. In the experiments conducted by Yoshinaga and Sato (1996), air and water served as the working fluid media, and ceramic spheres were used as solid particles. The density of air was determined using the ideal gas equation of state. The specific parameters of the experiment are listed in Table 2.

Table 2. Detailed parameters of Yoshinaga and Sato's experiment.

Parameter	Value	Parameter	Value
Pipe diameter	0.026 m	Pipe length	6.74 m
Solid density	2540 kg/m^3	Solid diameter	0.0061 m
Liquid density	1000 kg/m^3	Liquid viscosity	0.001 Pa·s

Figure 2 compares the model-predicted solid phase velocity with the experimentally measured results under different gas and liquid superficial velocities. The results indicate that, under both test conditions, the average relative error for the solid phase velocity does not exceed 5%, with a maximum relative error of 16.8%. This demonstrates a good agreement between the model-predicted solid phase velocity and the experimentally measured values.

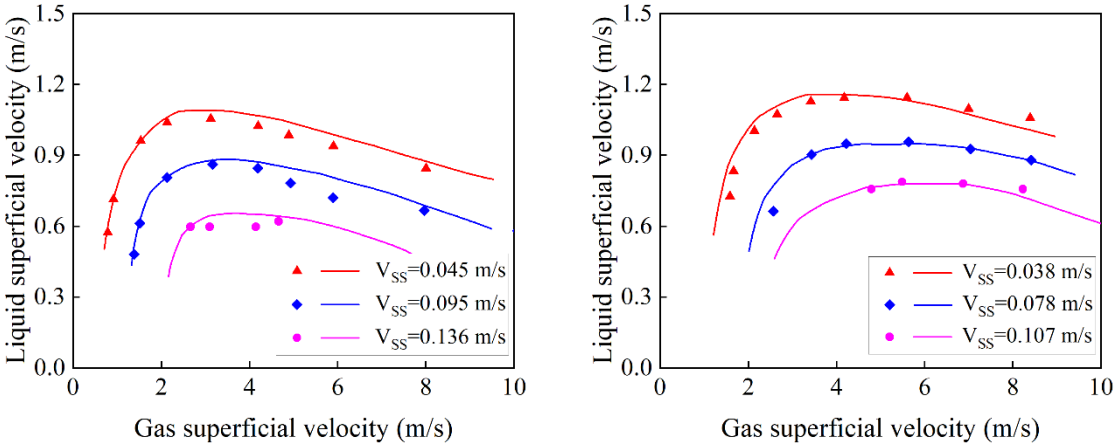

(**a**) Model comparison under first test (**b**) Model comparison under second test

Figure 2. A comparison between the measured solid velocity and predicted solid velocity using the proposed model.

2.2. Establishment of Automated Gas Influx Handling Model

2.2.1. Establishment of Automatic Adjustment Model of Choke Opening

Currently, over 90% of automatic control systems in the industry are implemented using PID controllers. The PID controller is widely used due to its simple algorithm, robustness, and high reliability. As shown in Figure 3, the PID controller consists of three components: the proportional part, the integral part, and the derivative part. Each of these serve the following functions: (1) the proportional part adjusts the deviation signal $e(t)$ proportionally, bringing it back to the normal proportional signal; (2) the integral part eliminates the deviations that occur during multi-stage signal transmission, improving the system's accuracy; (3) the derivative part introduces an effective initial correction signal in the system to control the deviation signal before it grows.

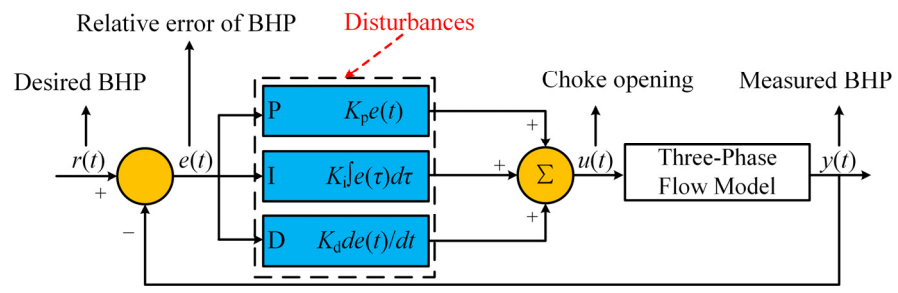

Figure 3. Schematic diagram of PID controller.

The automatic adjustment model of choke opening is established based on PID control theory, and its algorithm can be expressed as follows:

$$u(t) = K_p e(t) + K_i \int_0^t e(t\prime)dt\prime + K_d \frac{de(t)}{dt} \tag{8}$$

where $u(t)$ is the control variable or output of the PID controller at time t, $e(t)$ is the error at time t, which is the difference between the setpoint (desired value) and the measured process variable, K_p is the proportional gain, K_i is the integral gain, and K_d is the derivative gain.

In this model, the derivative part of the PID controller is neglected, so Equation (8) can be expressed as follows:

$$u(t) = u(t-1) + K_p[e(t) - e(t-1)] + K_i \frac{e(t) + e(t-1)}{2} \tag{9}$$

where $u(t)$ is the choke opening, $e(t)$ is the relative difference between the actual BHP and the target BHP, and K_p and K_i are the proportional and integral parameters of the PID controller, respectively.

The pressure drop generated by the gas–liquid–solid flow through the choke is calculated using the following [29]:

$$Q = \frac{C_v Z \sqrt{\max\left(P_{\text{top}} - P_S, 0\right)}}{x_{L-S} / \sqrt{\rho_{L-S,\text{top}}} + x_G / \left(Y \sqrt{\rho_{G,\text{top}}}\right)} \tag{10}$$

where Q is the total mass flow rate through the choke in kg/s, C_v is the inherent constant of the choke, Z is the choke opening, P_{top} is the pressure at the choke, in Pa, P_S is the downstream pressure of the choke, in Pa, x_{L-S} is the mass flow fraction of the liquid–solid mixture, x_G is the mass flow fraction of the gas phase, $\rho_{L-S,\text{top}}$ is the density of the liquid–solid mixture at the wellhead, in kg/m^3, $\rho_{G,\text{top}}$ is the density of the gas phase at the wellhead, in kg/m^3, and Y is the gas expansion factor (in this paper, $Y = 0.15$).

2.2.2. The Effect of Controller Parameters on Automated Gas Influx Handling

The input data of the well are summarized in Table 3. The parameters set for the simulated well in this study do not correspond to a real well but are instead carefully selected simulation parameters. This approach minimizes the complexity introduced by additional variables, thereby simplifying data analysis and allowing us to focus more directly on the core objectives of the study.

Table 3. Input data for the simulated well.

Parameter	Value	Parameter	Value
Well depth	4000/6000/8000 m	Drillpipe ID	0.0943 m
Drillpipe OD	0.1143 m	Bit diameter	0.1651 m
Drilling fluid volumetric flow rate	23.33/26.25/39.17 kg/s	Formation permeability	15/30/45 mD
Gas formation height	5 m	Gas formation radius	150 m
Drilling fluid inlet temperature	20 °C	Geothermal gradient	0.02 °C/m
ROP	20 m/h	Cuttings diameter	0.005 m
Drilling fluid viscosity	0.07 Pa·s	Wellbore roughness	25.4×10^{-6} m
Cuttings density	2650 kg/m^3	Drilling fluid density	1750 kg/m^3
Initial BHP difference	3 MPa	Pit gain alarm value	1/2.5/4 m^3

The parameters in the PID controller have a limited range of applicability. Exceeding this range can affect the control of BHP, potentially leading to formation fracturing or secondary gas influx, resulting in the failure of automated gas influx handling operations.

Figure 4 illustrates the effect of different proportional parameters (K_p = 0.2, 2, 8) on the automated gas influx handling with the same integral parameter (K_i = 0.001). As K_p increases, the time required for the BHP to rise to the formation pore pressure decreases. The times for the BHP to reach the pore pressure with different K_p values (0.2, 2, and 8) are 1820 s, 980 s, and 965 s, respectively. When K_p = 2, the controller effectively controls the BHP, allowing it to rise into the safe pressure window quickly. As K_p decreases, the response to BHP deviation weakens. When K_p = 0.2, the BHP exceeds the formation fracture pressure after 2390 s, causing formation fracturing. If K_p is set too high, the controller's response to BHP deviations becomes too strong, leading to oscillations in BHP. When K_p = 8, after the BHP rises to the formation pore pressure, oscillations occur, resulting in formation fracturing and secondary gas influx.

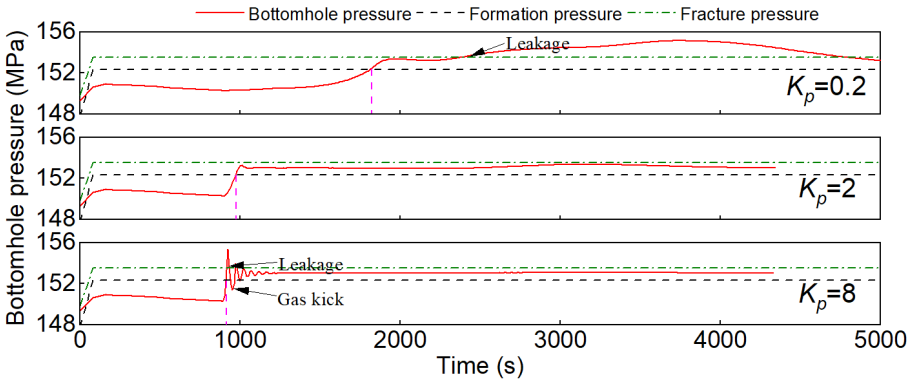

Figure 4. BHP vs. time during automatic gas kick attenuation with different K_p (Black dashed line represents formation pressure, and the green dashed line represents fracture pressure).

Figure 5 illustrates the effect of different integral parameters (K_i = 0.001, 0.01, 0.2) on the automated gas influx handling with the same proportional parameter (K_p = 2). The value of K_i has little impact on the time to restore the BHP. When K_i = 0.01, the controller effectively controls the BHP, allowing it to quickly rise into the safety pressure window. If K_i decreases to 0.001, after the BHP exceeds the pore pressure, the controller's ability to control the BHP weakens, reducing the difference between the BHP and the formation fracture pressure. After the gas influx stops, the minimum difference between the formation fracture pressure and the BHP is 0.179 MPa and 0.164 MPa for K_i = 0.01 and K_i = 0.001, respectively. If K_i increases to 0.2, the BHP exceeds the formation fracture pressure during gas influx handling, causing formation fracturing.

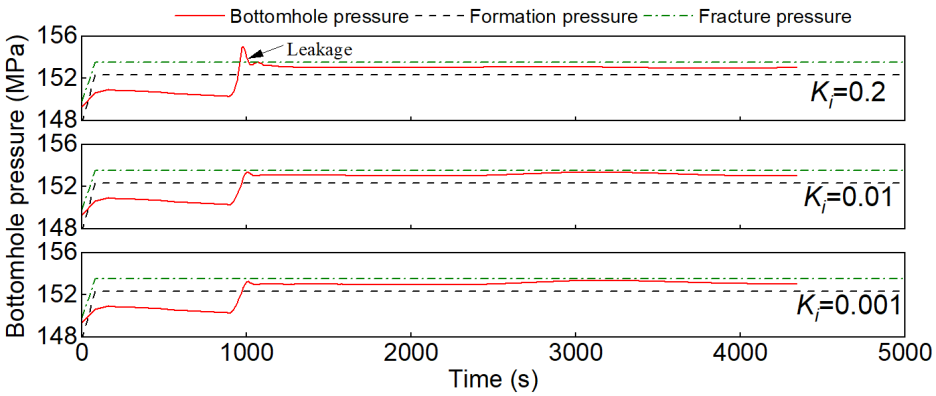

Figure 5. BHP vs. time during automatic gas kick attenuation with different K_i (Black dashed line represents formation pressure, and the green dashed line represents fracture pressure).

2.2.3. Comparison of Automated Method and Traditional Methods in Gas Influx Handling

The results of gas influx handling using the automated method and traditional methods (the DM and the WWM) are compared. The well depth, formation permeability, initial BHP differential, pit gain alarm value, and drilling fluid volumetric flow rate are set to 8000 m, 30 mD, 3 MPa, 2.5 m^3, and 26.25 kg/s, respectively. The drilling fluid used is WBDF.

Figure 6 shows that the variation curves of pit volume increase over time during gas influx handling with WBDF using the three methods. All three methods reach the pit gain alarm value at around 670 s. After 670 s, the rate of pit volume increase slows down for the automated method; as the choke opening starts to decrease automatically, the choke pressure increases, and the pressure difference between the bottomhole and the formation decreases, resulting in a reduced rate of gas influx from the formation into the wellbore. For the DM and the WWM, after reaching the pit gain alarm value, the pit volume continues to increase at a similar rate for a certain period. This is because, for both the DM and the WWM, some time is required to conduct a flow check and shut in the well (in this comparison, the total time for flow check and shut-in is set to 200 s). After shut-in, the BHP increases, reducing the gas influx rate and slowing the pit volume increase. Once the gas influx from the formation stops, the pit volume continues to increase due to the expansion of the gas as it rises in the wellbore. The maximum pit volume increase for the three gas influx handling methods (DM, WWM, and automated method) is 8.10 m^3, 8.10 m^3, and 7.88 m^3, respectively.

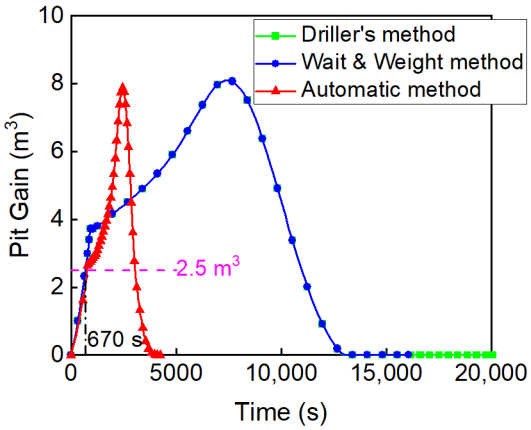

Figure 6. Pit gain vs. time for the automatic method, DM, and WWM. (Note: The curves for DM and WWM appear nearly identical due to their close values, resulting in an apparent overlap. Careful inspection along the *X*-axis reveals all three curves.)

Figure 7 shows the variation curves of choke/casing pressure over time for the three methods. The time required from the detection of gas influx to the completion of handling for the automated method, DM, and WWM is 4250 s, 45,073 s, and 30,153 s, respectively. This means that the time required for the automated method is approximately 10% of the DM and about 14.3% of the WWM. This is because, during automated gas influx handling, the drilling fluid pump volumetric flow rate remains the same as during normal drilling, allowing the intruded gas to be circulated out of the well more quickly. In contrast, when using the DM or WWM, the pump volumetric flow rate is only 25% to 50% of the normal drilling rate.

The maximum choke/casing pressure during gas influx handling with the automated method is lower than that of the DM and WWM. The maximum choke/casing pressure is reached at 2510, 7680, and 7680 s for the automated method, DM, and WWM, respectively, with the corresponding maximum pressures being 16.52, 23.08, and 23.08 MPa. Compared to the DM and WWM, the automated method reduces the maximum choke/casing pressure by 6.56 MPa (a reduction of 28.42%).

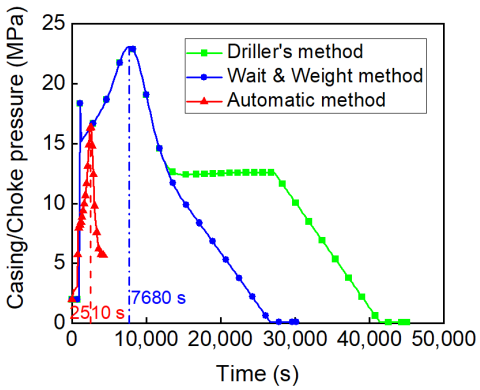

Figure 7. Choke/casing pressure vs. time for the automatic gas kick attenuation method, DM, and WWM after gas kick in WBDF.

Figure 8 shows the composition of BHP and the cuttings volume fraction profile at the time of maximum casing/choke pressure for the DM and the automated method. At the time of maximum casing/choke pressure, the annular gas–liquid–solid phase gravity pressure drop for the DM and the automated method is 128.15 MPa and 128.36 MPa, respectively, meaning the annular fluid gravity pressure drop for the automated method is 0.21 MPa higher than that of the DM, accounting for 3.20% of the reduction in the maximum choke/casing pressure (6.56 MPa). This is primarily because, during gas influx handling with the DM, drilling is stopped, and no cuttings are present in the lower part of the annulus. In contrast, with the automated method, drilling continues during gas influx handling, resulting in cuttings being present throughout the entire wellbore (Figure 8b), which causes the gravity pressure drop from cuttings in the automated method to be higher than in the DM. As shown in Figure 8a, the annular frictional pressure drop in the automated method is 6.30 MPa higher than in the DM, accounting for 96.04% of the reduction in maximum choke/casing pressure (6.56 MPa). This is because the pump volumetric flow rate during gas influx handling with the automated method is the same as during normal drilling, resulting in a high annular flow rate and a larger annular frictional pressure drop. Therefore, the main reason the automated method can effectively reduce the maximum choke/casing pressure is the higher annular frictional pressure drop during gas influx handling. The secondary reason is the higher gravity pressure drop from cuttings in the annulus.

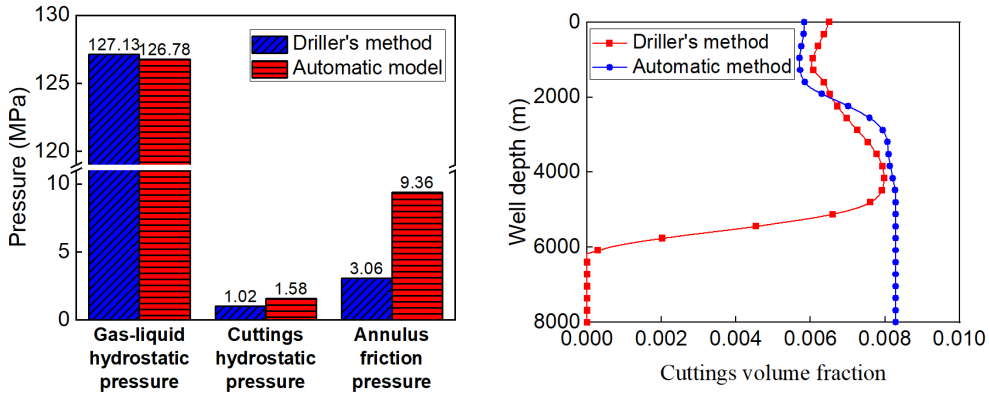

(**a**) Comparison of pressure drop component (**b**) Comparison of cuttings volume fraction

Figure 8. Wellbore pressure compositions and cuttings volumetric fraction profiles when choke/casing pressure reaches its maximum for DM and automatic method.

Figure 9 shows the variation in the cuttings volume fraction profile during gas influx handling with WBDF using the DM and the automated method. At the initial time, the cuttings volume fraction throughout the annulus is 0.0083 (0 s). As gas invades, due to

the presence of free gas, the cuttings volume fraction at the bottomhole decreases (500 s). After the gas influx stops, the cuttings volume fraction at the bottomhole for the automated method returns to 0.0083 (1000 s), while for the DM, the cuttings volume fraction drops to 0 (1500 s). This is because, during gas influx handling, the automated method does not stop drilling, while the DM halts drilling. Once the gas is fully circulated out of the well, the cuttings volume fraction throughout the entire wellbore returns to 0.0083 for the automated method, whereas for the DM, the cuttings volume fraction throughout the wellbore becomes 0.

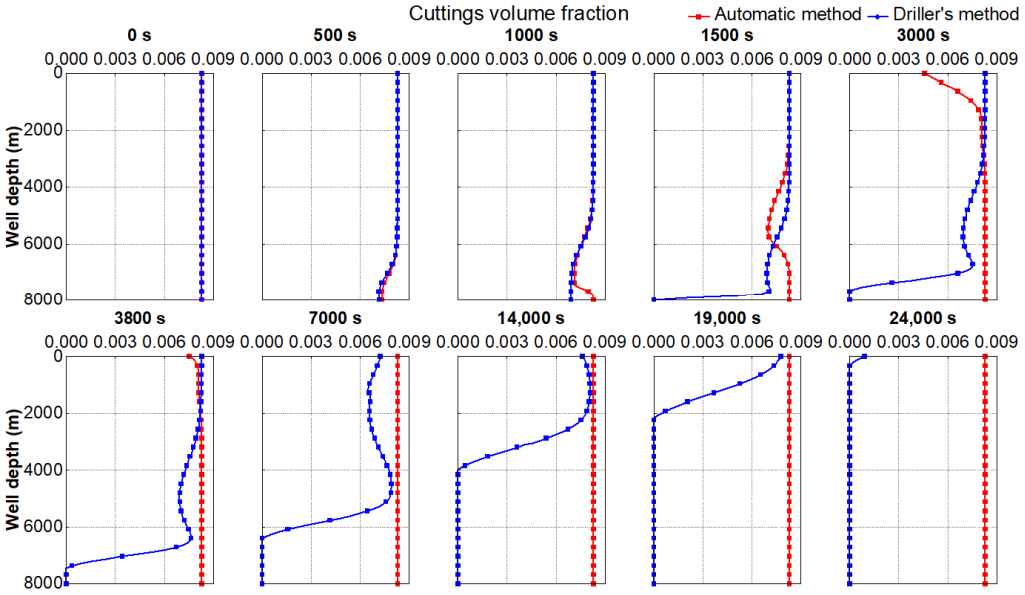

Figure 9. Cuttings volumetric fraction profiles after gas kick in WBDF for DM and automatic gas kick attenuation method.

3. Sensitivity Analysis of Automated Gas Influx Handling Mechanisms

3.1. Effect of Gas Solubility

The results of gas influx handling using the automated method for WBDF and OBDF are compared. The well depth, formation permeability, initial BHP differential, pit gain alarm value, and drilling fluid volumetric flow rate are set to 8000 m, 30 mD, 3 MPa, 2.5 m^3, and 26.25 kg/s, respectively.

Figure 10 shows the gas-phase volume fraction profiles at different times during gas influx handling using the automated method for WBDF and OBDF. Since the gas solubility in WBDF is negligible, free gas starts to appear at the bottomhole early in the gas influx. In contrast, for OBDF, the invaded gas remains in the form of dissolved gas in the annulus for a longer period during the early stages of gas influx. At 2130 s, the dissolved gas in the OBDF begins to separate out, with the gas release occurring at well depths between 1120 m and 1600 m.

Figure 11 shows the time-dependent variation curves of BHP during gas influx handling using the automated method for WBDF and OBDF. The time required to handle gas influx in WBDF and OBDF is 4250 s (70.8 min) and 5550 s (92.5 min), respectively, meaning the gas influx handling time for WBDF is 75% of that for OBDF. This is because the invaded gas exists in the form of free gas in WBDF, and due to the slip between the free gas phase and the liquid phase, the transport speed of free gas in the annulus is greater than that of the WBDF. In contrast, in OBDF, the invaded gas mostly exists as dissolved gas in the wellbore, and the speeds of dissolved gas and OBDF are same. Therefore, it takes longer to circulate all the invaded gas out of the wellbore in OBDF.

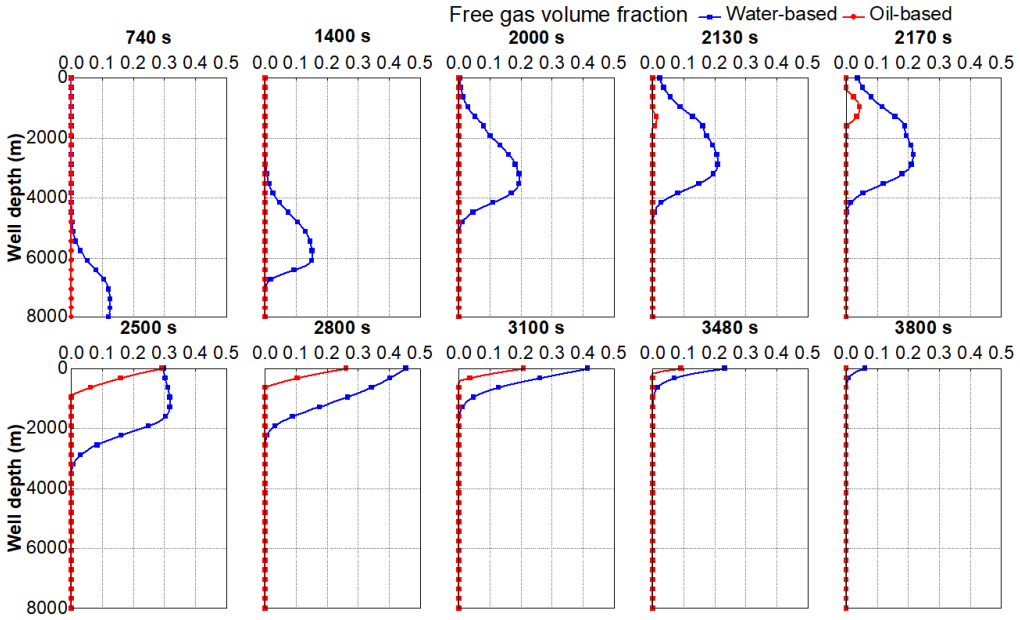

Figure 10. Free gas volumetric fraction profiles during automatic gas kick attenuation in WBDF and OBDF.

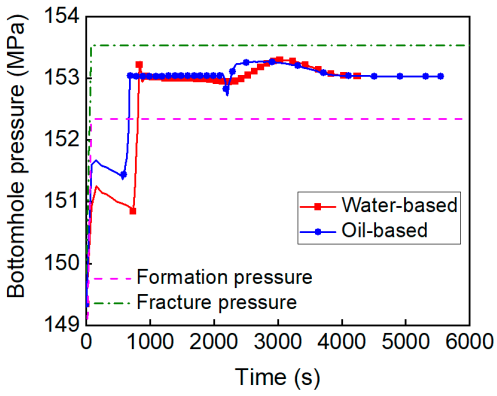

Figure 11. BHP vs. time after gas kick in WBDF and OBDF for automatic handling method.

Figure 12a shows the variation curves of pit volume increase during gas influx handling using the automated method for WBDF and OBDF. The time required to reach the pit gain alarm value is 730 s for WBDF and 570 s for OBDF, meaning the time for OBDF to reach the alarm value is 80% of that for WBDF. This is because, in the HTHP environment at the bottomhole, the invaded gas causes a greater increase in the volume of OBDF compared to the volume occupied by free gas in WBDF, allowing OBDF to reach the pit gain alarm value more quickly. Figure 12b shows the gas-phase volume fraction profile in WBDF and the formation volume factor profile in OBDF at the time they each reach the pit gain alarm value. At the bottomhole, the gas-phase volume fraction in WBDF is 0.12, while the formation volume factor for OBDF is 1.31, indicating that the volume increase for OBDF is 0.31.

As seen in Figure 12a, the maximum pit volume increases for WBDF and OBDF are 7.88 m^3 and 3.22 m^3, respectively, meaning the maximum pit volume increase in OBDF is about 40% of that in WBDF. This is because, in OBDF, the invaded gas exists as dissolved gas in the lower part of the wellbore, and as it is transported to the wellhead with the OBDF, only a small portion of the dissolved gas separates out as free gas, which contributes only a small increase to the pit volume.

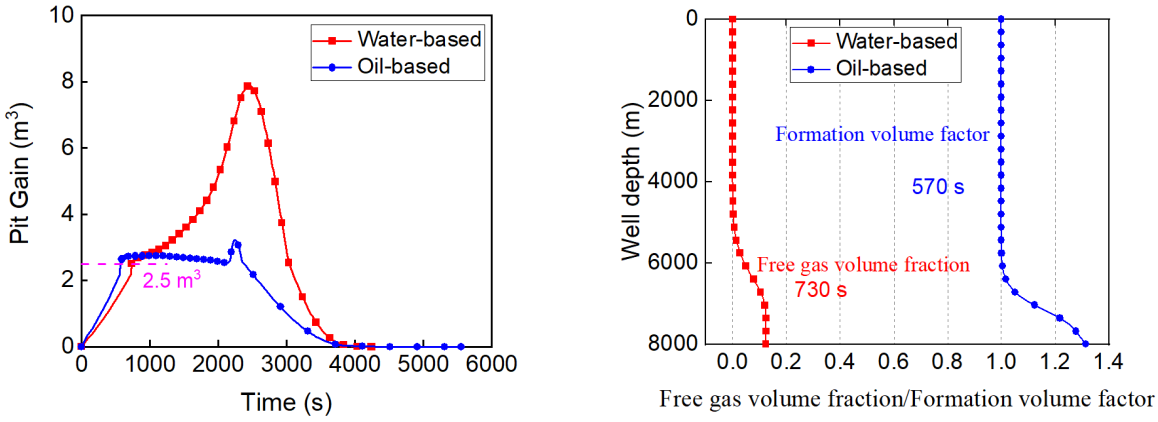

(**a**) Pit gain vs. time for WBDF and OBDF (**b**) Gas fraction and formation volume factor profiles

Figure 12. Pit gain, free gas volumetric fraction, and formation volume factor during automatic gas kick attenuation in WBDF and OBDF.

Figure 13 shows the free gas-phase volume fraction profile for WBDF at the time of maximum pit volume increase, as well as the free gas-phase volume fraction and solubility profiles for OBDF at the time of its maximum pit volume increase. In OBDF, the free gas begins to separate out at a well depth of 1360 m. The free gas-phase volume fractions at the wellhead for WBDF and OBDF are 0.26 and 0.20, respectively.

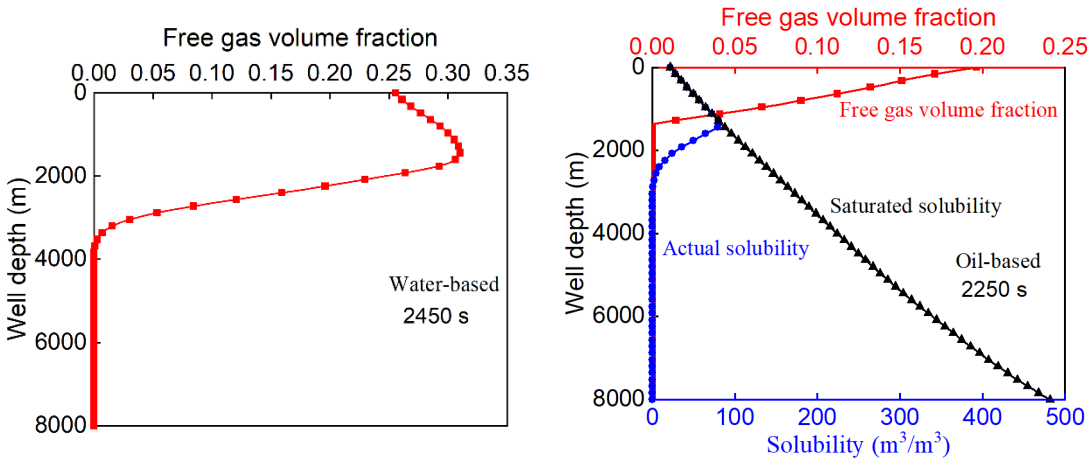

(**a**) Free gas volume fraction profile (**b**) Gas fraction and solubility profiles

Figure 13. Free gas volumetric fraction profiles and gas solubility profiles when the pit gain reaches its maximum in WBDF and OBDF.

Additionally, at the time of maximum pit volume increase, the volume of displaced liquid phase in WBDF is greater than that in OBDF. As a result, the choke pressure required to maintain constant BHP in WBDF is higher than that required in OBDF. As shown in Figure 14, the maximum choke pressures for WBDF and OBDF are 16.52 MPa and 9.64 MPa, respectively, meaning the maximum choke pressure required for OBDF is about 60% of that for WBDF. After the invaded gas is circulated out of the well, the choke pressures required for both WBDF and OBDF become equal.

As shown in Figure 15, after 2100 s, the choke openings for both WBDF and OBDF increase rapidly, but the rate of increase is faster for OBDF. This is because the dissolved gas in OBDF suddenly separates out near the wellhead, causing the flow rate through the choke to increase more rapidly than in WBDF. Therefore, the choke opening must be increased quickly to prevent excessive choke pressure and maintain constant BHP.

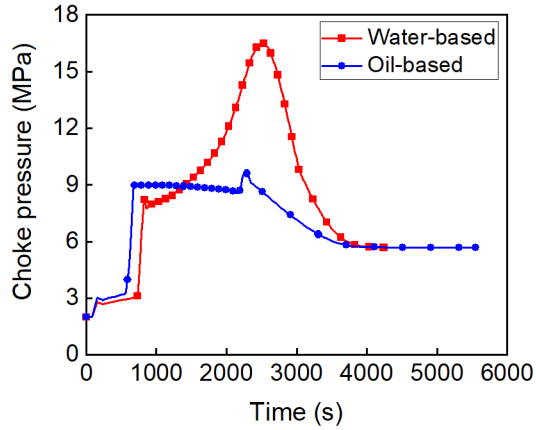

Figure 14. Choke pressure vs. time after gas kick in WBDF and OBDF for automatic gas kick attenuation method.

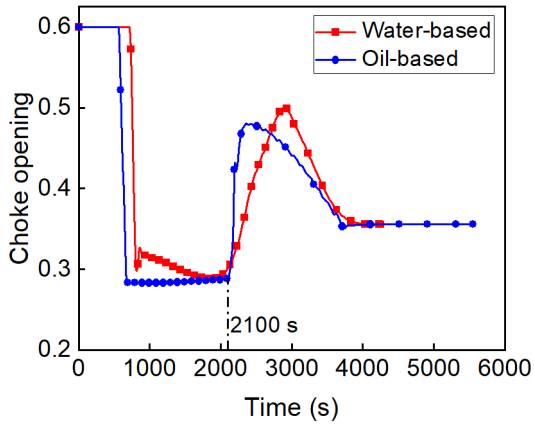

Figure 15. Choke opening vs. time after gas kick in WBDF and OBDF for automatic gas kick attenuation method.

3.2. Effect of Well Depth

The formation permeability, initial BHP differential, pit gain alarm value, and drilling fluid volumetric flow rate are set to 30 mD, 3 MPa, 2.5 m^3, and 26.25 kg/s, respectively.

Figure 16 shows the variation curves of pit volume increase and gas mass flow rate over time during gas influx handling using the automated method for different well depths in WBDF. As shown in Figure 16a, the maximum pit volume increases for WBDF at different well depths (4000 m, 6000 m, and 8000 m) are 5.93 m^3, 7.26 m^3, and 7.96 m^3, respectively. The maximum pit volume increase in WBDF increases with well depth. From 4000 m to 6000 m, the maximum pit volume increase rises by 18.32%, and from 6000 m to 8000 m, it increases by 8.79%. This is because, as the well depth increases, the BHP also increases, leading to an increase in gas density at the bottomhole. Therefore, at the same pit gain alarm value, the wellbore at greater depth contains a larger mass of invaded gas (Figure 16b; the total masses of invaded gas for 4000 m, 6000 m, and 8000 m are 1239.9 kg, 1701.0 kg, and 1980.5 kg, respectively). This results in a larger volume of displaced drilling fluid after the expansion of free gas, leading to an increase in the maximum pit volume increase.

Figure 17 shows the variation curves of pit volume increase and gas mass flow rate over time during gas influx handling using the automated method for different well depths in OBDF. As shown in Figure 17a, the maximum pit volume increases in OBDF at different well depths (4000 m, 6000 m, and 8000 m) are 3.84 m^3, 3.59 m^3, and 3.32 m^3, respectively. The maximum pit volume increase in OBDF decreases with increasing well depth. From 4000 m to 6000 m, the maximum pit volume increase decreases by 6.51%, and from 6000 m to 8000 m, it decreases by 7.52%. This is because, as well depth increases, the wellbore

pressure also increases, causing the formation volume factor of the OBDF to increase. As a result, at the same pit gain alarm value, the wellbore at greater depth contains less invaded gas mass. This leads to a smaller volume of displaced drilling fluid after the expansion of the OBDF and the gas separation, resulting in a reduction in the maximum pit volume increase.

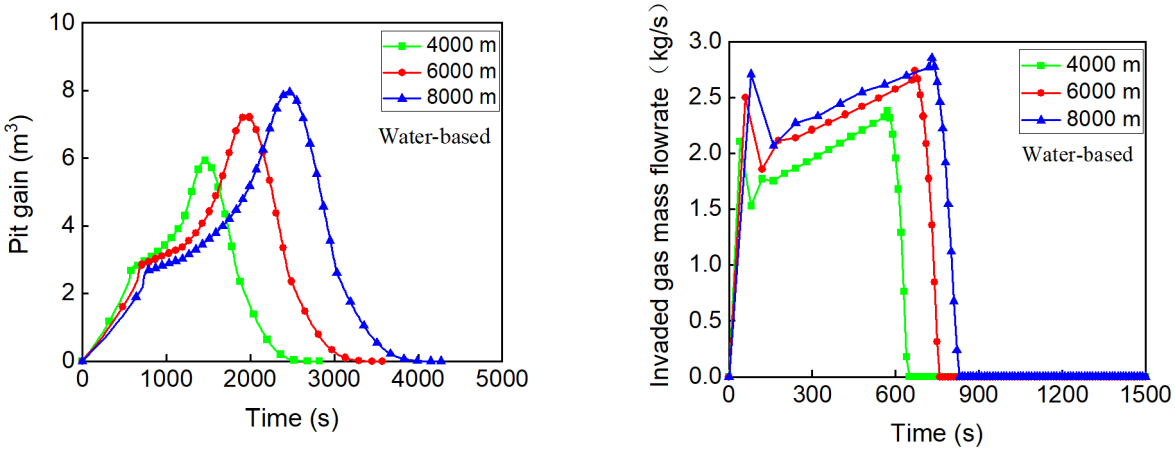

(**a**) Pit gain under different well depths for WBDF (**b**) Invaded gas rate under different depths for WBDF

Figure 16. Pit gain and gas influx mass rate vs. time during automatic gas kick attenuation in WBDF under different well depths.

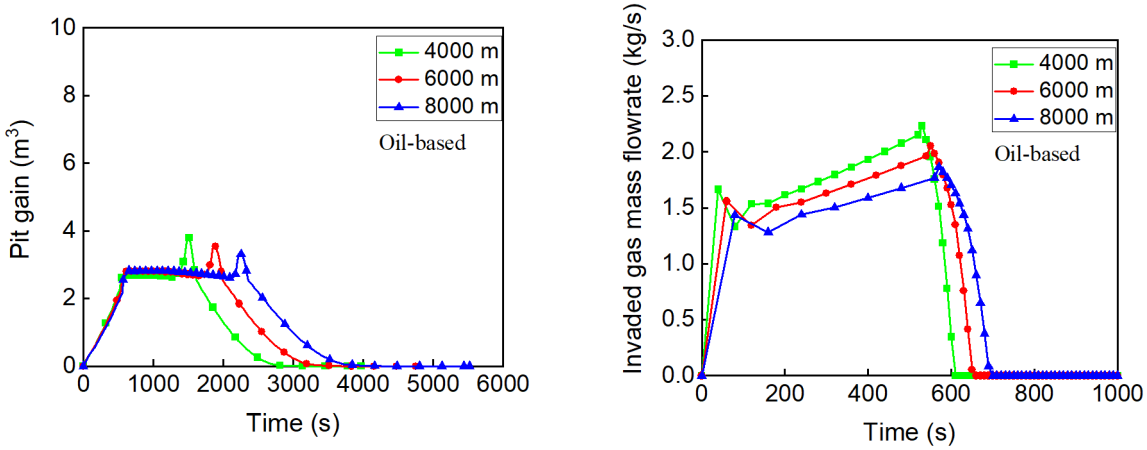

(**a**) Pit gain under different depths for OBDF (**b**) Invaded gas rate under different depths for OBDF

Figure 17. Pit gain and gas influx mass rate vs. time during automatic gas kick attenuation in OBDF under different well depths.

Figure 18 shows the variation curves of choke pressure over time during gas influx handling in WBDF and OBDF. For WBDF, the maximum choke pressures at different well depths (4000 m, 6000 m, and 8000 m) are 14.18 MPa, 15.80 MPa, and 16.61 MPa, respectively. From 4000 m to 6000 m, the maximum choke pressure increases by 10.25%, and from 6000 m to 8000 m, it increases by 4.88%. This is because, as the well depth increases, the volume of displaced liquid phase in WBDF increases, which in turn raises the choke pressure required to maintain constant BHP.

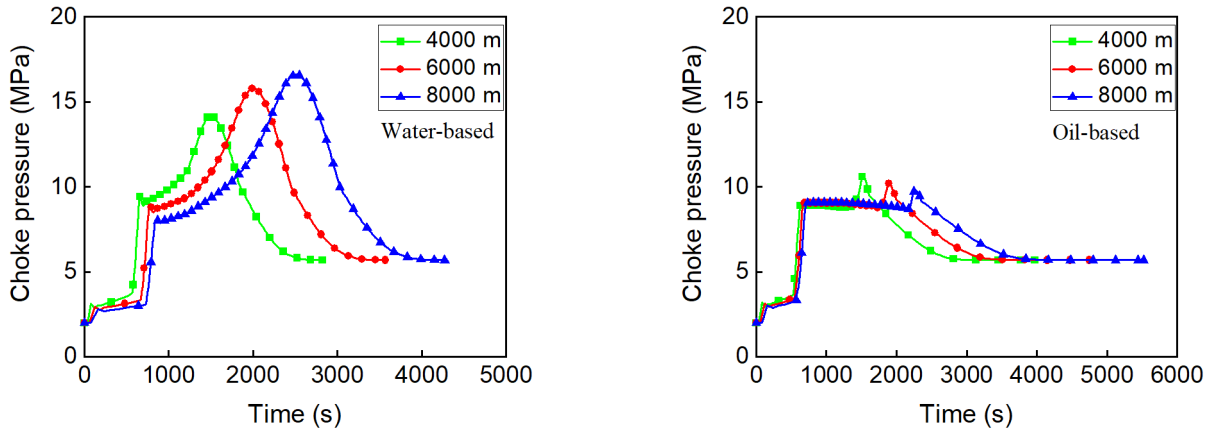

(**a**) Choke pressure under different depths for WBDF (**b**) Choke pressure under different depths for OBDF

Figure 18. Choke pressure vs. time during automatic gas kick attenuation in WBDF and OBDF under different well depths.

For OBDF, the maximum choke pressures at different well depths (4000 m, 6000 m, and 8000 m) are 10.67 MPa, 10.21 MPa, and 9.77 MPa, respectively. From 4000 m to 6000 m, the maximum choke pressure decreases by 4.31%, and from 6000 m to 8000 m, it decreases by 4.31%. This is because, as the well depth increases, the volume of displaced liquid phase in OBDF decreases, leading to a reduction in the choke pressure required to maintain constant BHP.

3.3. Effect of Gas Influx Volume

The well depth, formation permeability, initial BHP differential, and drilling fluid volumetric flow rate are set to 8000 m, 30 mD, 3 MPa, and 26.25 kg/s, respectively. Figure 19 illustrates the effect of gas influx volume on BHP during gas influx handling in WBDF using the automated method. As the gas influx volume increases (1.0 m^3, 2.5 m^3, and 4.0 m^3), the time to start handling the gas influx is delayed (330 s, 730 s, and 1130 s), and the corresponding BHP at the start of handling is lower (151.06 MPa, 150.85 MPa, and 150.59 MPa). Additionally, the time required to circulate all the intruded gas out of the well increases (3890 s, 4270 s, and 4590 s).

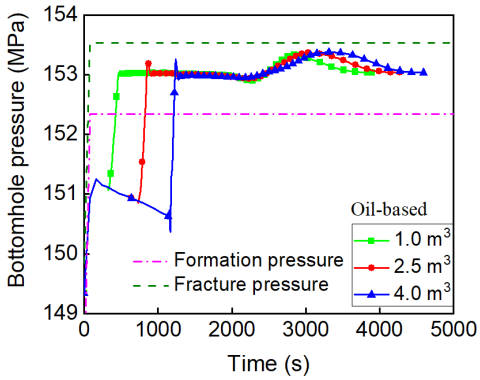

Figure 19. BHP vs. time during automatic gas kick attenuation in WBDF under different gas kick sizes.

Figure 20 illustrates the effect of gas influx volume on choke opening and choke pressure during gas influx handling in WBDF using the automated method. As shown in Figure 20a, with the increase in gas influx volume (1.0 m^3, 2.5 m^3, and 4.0 m^3), the minimum choke opening decreases (0.312, 0.288, and 0.273). This is because, as the gas influx volume increases, the volume of displaced drilling fluid also increases, resulting in

a decrease in the annular fluid gravity pressure drop. Consequently, the choke pressure needs to be increased to maintain constant BHP (Figure 20b), leading to a reduction in the choke opening. As the gas influx volume increases, the maximum choke opening also increases (0.475, 0.498, and 0.506). This is because, with a larger gas influx volume, the fluid volumetric flow rate through the choke increases, requiring a larger choke opening to maintain constant BHP and avoid generating excessive BHP.

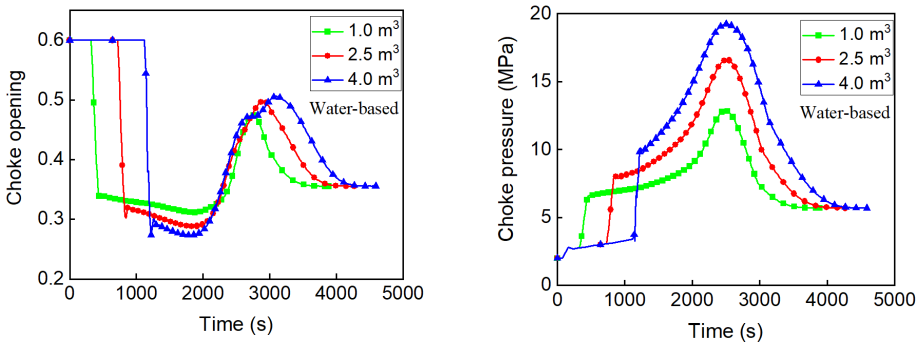

(**a**) Choke opening under different gas kick sizes (**b**) Choke pressure under different gas kick sizes

Figure 20. Choke opening and choke pressure vs. time during automatic gas kick attenuation in WBDF under different gas kick sizes.

3.4. Effect of Formation Permeability

The well depth, gas influx volume, initial BHP differential, and drilling fluid volumetric flow rate are set to 8000 m, 2.5 m^3, 3 MPa, and 26.25 kg/s, respectively. Figure 21 shows the variation curves of pit volume increase, BHP, choke opening, and choke pressure over time during gas influx handling in WBDF using the automated method under different formation permeability conditions. As the formation permeability increases, the time required to reach the pit gain alarm value becomes shorter, and the maximum pit volume increase also rises. Under different formation permeability conditions (20 mD, 30 mD, and 40 mD), the times to reach the pit gain alarm value are 890 s, 730 s, and 725 s, respectively, with corresponding maximum pit volume increases of 7.86 m^3, 7.96 m^3, and 8.55 m^3. This occurs because, as formation permeability increases, the mass of gas intruding into the wellbore during the period when the choke opening automatically decreases to restore BHP balance also increases, leading to a larger maximum pit volume increase. The total masses of gas intruding into the wellbore under different formation permeability conditions (20 mD, 30 mD, and 40 mD) are 1980.5 kg, 2047.3 kg, and 2194.3 kg, respectively.

As shown in Figure 21c, when the intruded gas migrates near the wellhead, the increase in choke opening becomes larger with higher formation permeability. After the gas influx, the maximum choke openings under different formation permeability conditions (20 mD, 30 mD, and 40 mD) are 0.492, 0.498, and 0.503, respectively. This is because, as formation permeability increases, the gas influx rate increases, raising the local gas-phase volume fraction in the annulus and, consequently, the gas-phase volume fraction flowing through the wellhead. This increases the fluid flow rate through the choke, requiring an increase in choke opening to prevent excessively high choke pressure that could cause formation fracturing, while maintaining constant BHP (Figure 21d).

3.5. Effect of Drilling Fluid Volumetric Flow Rate

The well depth, gas influx volume, formation permeability, and initial BHP differential are set to 8000 m, 2.5 m^3, 30 mD, and 2 MPa, respectively. As shown in Figure 22, with the increase in drilling fluid volumetric flow rate (23.33 kg/s, 26.25 kg/s, and 29.17 kg/s), the time to start handling the gas influx is delayed (660 s, 730 s, and 1060 s), and the corresponding BHP at the start of handling is higher (150.49 MPa, 150.85 MPa, and 151.29 MPa). Additionally, the time required to circulate all the gas out of the well decreases (4510 s,

4270 s, and 4190 s). This is because, as the volumetric flow rate increases, the frictional pressure drop increases, reducing the pressure difference between the bottomhole and the formation, which in turn slows the gas influx rate, resulting in a longer time to reach the pit gain alarm value. At a higher drilling fluid volumetric flow rate, the gas velocity increases, reducing the gas influx handling time.

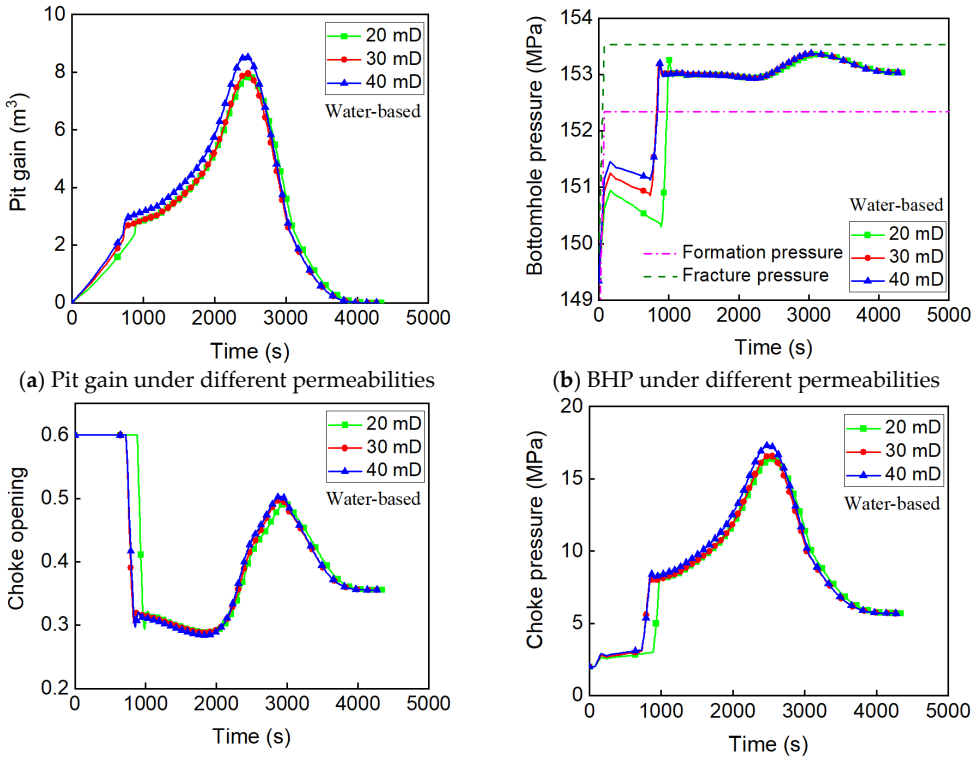

(**a**) Pit gain under different permeabilities (**b**) BHP under different permeabilities

(**c**) Choke opening under different permeabilities (**d**) Choke pressure under different permeabilities

Figure 21. Pit gain, BHP, choke opening, and choke pressure vs. time during automatic gas kick attenuation in WBDF under different formation permeability.

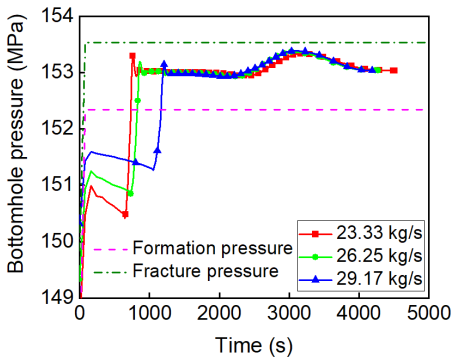

Figure 22. BHP vs. time during automatic gas kick attenuation under different drilling fluids volumetric flow rates.

As shown in Figure 23, at the early stage of gas influx, the gas-phase volume fraction at the bottomhole decreases as the drilling fluid volumetric flow rate increases. At 640 s, the gas-phase volume fractions at the bottomhole under different drilling fluid volumetric flow rates (23.33 kg/s, 26.25 kg/s, and 29.17 kg/s) are 0.158, 0.116, and 0.071, respectively. This is because, with the increased drilling fluid volumetric flow rate, the apparent volumetric flow rate of the liquid phase increases, leading to a larger portion of the annular cross-sectional area being occupied by the liquid phase, thereby reducing the gas-phase volume fraction. The higher the drilling fluid volumetric flow rate, the faster the invaded gas migrates

through the wellbore. At 1900 s, under a drilling fluid volumetric flow rate of 29.17 kg/s, the gas has already reached the wellhead, while under 23.33 kg/s and 26.25 kg/s, the gas has not yet reached the wellhead. This is due to the increased liquid-phase velocity with higher drilling fluid volumetric flow rate, which also increases the gas-phase velocity, speeding up gas migration through the wellbore. Additionally, the maximum gas-phase volume fraction at the wellhead decreases as the drilling fluid volumetric flow rate increases. The maximum gas-phase volume fractions at the wellhead under different drilling fluid volumetric flow rates (23.33 kg/s, 26.25 kg/s, and 29.17 kg/s) are 0.50, 0.47, and 0.42, respectively.

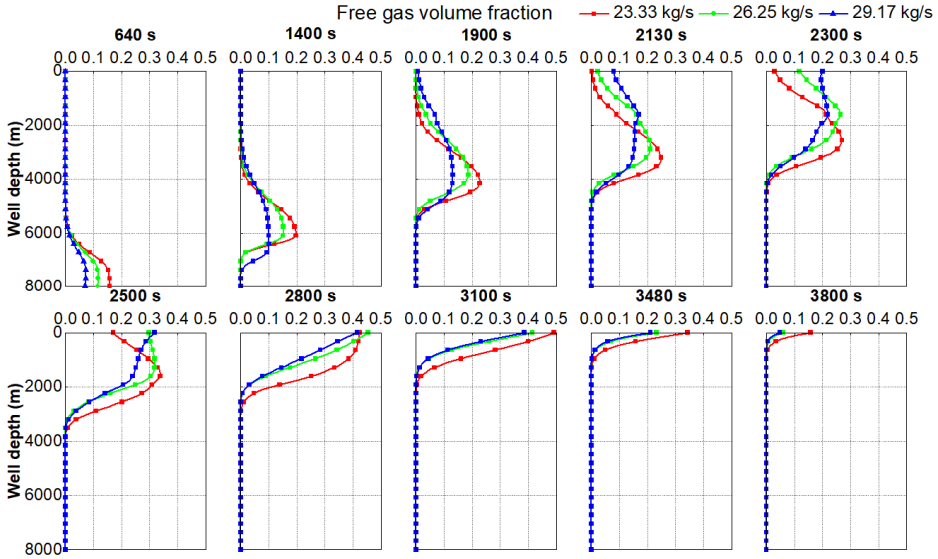

Figure 23. Gas volumetric fraction profiles at different time during automatic gas attenuation under different drilling fluids volumetric flow rates.

Figure 24 shows the variation curves of pit volume increase over time under different drilling fluid volumetric flow rates. As the drilling fluid volumetric flow rate increases (23.33 kg/s, 26.25 kg/s, and 29.17 kg/s), the maximum pit volume increase decreases (8.91 m^3, 7.96 m^3, and 7.13 m^3). This is because the increase in drilling fluid volumetric flow rate leads to a greater annular frictional pressure drop, which raises the BHP and reduces the gas influx rate, thereby decreasing the maximum pit volume increase.

As the drilling fluid volumetric flow rate increases, the BHP increases, and the gas influx rate into the wellbore decreases. As a result, the choke pressure required to maintain constant BHP decreases (Figure 25a), leading to an increase in the minimum choke opening (Figure 25b). Under different drilling fluid volumetric flow rates (23.33 kg/s, 26.25 kg/s, and 29.17 kg/s), the maximum choke pressures are 19.00 MPa, 16.61 MPa, and 14.13 MPa, respectively, while the minimum choke openings are 0.271, 0.288, and 0.309, respectively.

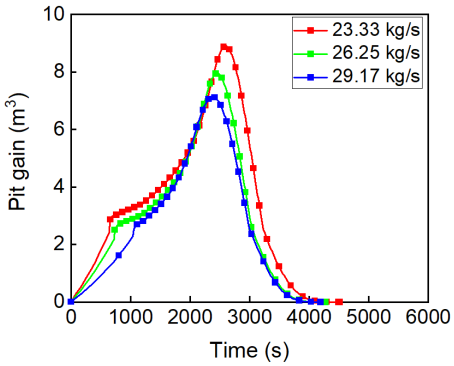

Figure 24. Pit gain vs. time during automatic gas kick attenuation under different drilling fluids volumetric flow rates.

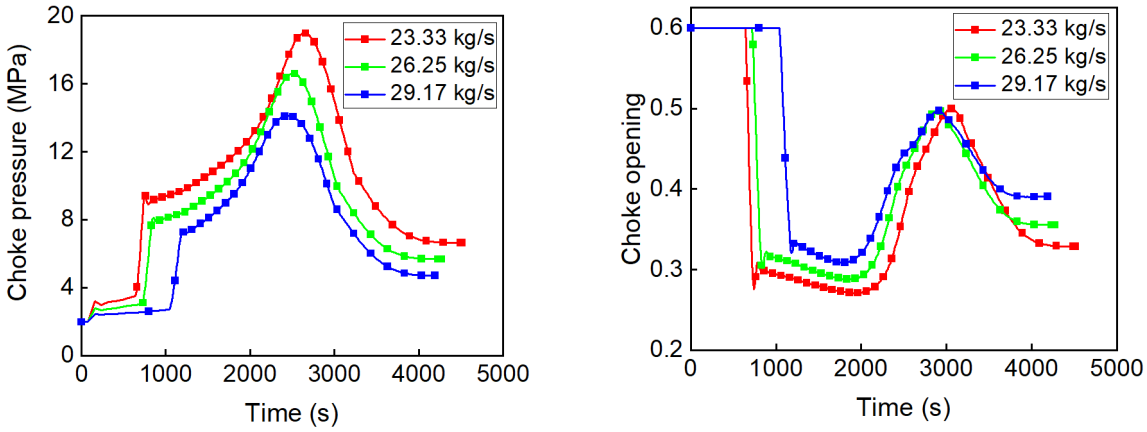

(**a**) Choke pressure under different drilling fluids volumetric flow rates

(**b**) Choke opening under different drilling fluids volumetric flow rates

Figure 25. Choke opening and choke pressure vs. time during automatic gas kick attenuation under different drilling fluids volumetric flow rates.

4. Conclusions

An efficient gas–liquid–solid flow model was developed using gas-phase drift and cuttings settling velocity models, achieving real-time BHP prediction. A PI-based choke adjustment model was compared with the DM and WWM for gas influx handling, with the following key findings:

(1) The model meets real-time prediction requirements with a grid number below 250 and a calculation time under 1/300th of simulated influx time.
(2) The automated method handles gas influx 10 times faster than DM and 7 times faster than WWM, reducing maximum choke pressure by 28.42% and safely managing larger influxes.
(3) Gas influx handling in WBDF is 75% faster than in OBDF due to free gas phase slip. The maximum choke pressure and pit volume increase with depth in WBDF but decrease in OBDF.
(4) Increasing gas influx, permeability, and pressure differential lowers the minimum choke opening, while raising the maximum choke opening and pressure.
(5) Higher drilling fluid flow rates raise the minimum choke opening, decrease the maximum choke opening, and reduce the choke pressure.

Author Contributions: Conceptualization, Y.Z. and Z.X.; methodology, J.L. and Z.D.; software, Z.X.; validation, Z.X., Y.Z. and W.Z.; formal analysis, J.L. and Z.D.; investigation, Y.Z.; resources, W.Z.; data curation, Z.X.; writing—original draft preparation, Y.Z.; writing—review and editing, Z.X.; visualization, W.Z.; supervision, Z.X.; project administration, Y.Z.; funding acquisition, W.Z. All authors have read and agreed to the published version of the manuscript.

Funding: This research was funded by Opening Funding of State Key Laboratory of Shale Oil and Gas Enrichment Mechanisms and Efficient Development grant number 35800000-23-ZC0613-0005.

Data Availability Statement: Dataset available on request from the authors.

Conflicts of Interest: Yanbin Zang and Wenping Zhang are employed by company. The remaining author declares that the research was conducted in the absence of any commercial or financial relationships that could be construed as a potential conflict of interest.

Nomenclature

Abbreviations	
API	API gravity of OBDF
BHP	bottomhole pressure
DM	driller's method
HTHP	High temperature and high pressure
MPD	managed pressure drilling
OBDM	oil-based drilling fluid
PI	proportional–integral
PID	proportional–integral–derivative
ROP	rate of penetration
WBDM	water-based drilling fluid
WWM	wait-and-weight method
Greek letters	
ρ	density, kg/m^3
α	volumetric fraction
θ	wellbore inclination, $^\circ$
γ	profile parameter reduction term
μ	fluid viscosity, Pa·s
$\rho_{L-S,\text{top}}$	density of the liquid–solid mixture at the wellhead, kg/m^3
$\rho_{G,\text{top}}$	density of the gas phase at the wellhead, kg/m^3
A	profile parameter for low gas fraction in liquid
C_0^{G-L}	distribution parameter between the gas and liquid phases
C_0^{S-L}	distribution parameter between the cuttings and the liquid phase
C_d	drag coefficient
C_v	inherent constant of the choke
d_*	dimensionless cuttings diameter
$e(t)$	error at time t, which is the difference between the setpoint (desired value) and the measured process variable
F_f	frictional pressure drop of the annular mixture, kg/m^2/s^2
g	gravitational acceleration, m/s^2
K	critical Kutateladze number
K_p	proportional gain
K_i	integral gain
K_d	derivative gain
m	gas, liquid, and solid phases (G, L, S)
P	pressure, Pa
P_{top}	pressure at the choke, Pa
P_S	downstream pressure of the choke, Pa
P_{bh}	actual bottomhole pressure, Pa
P_{bh}^{ref}	desired bottomhole pressure, Pa
P_c^{ref}	desired choke pressure, Pa
Q	total mass flow rate through the choke, kg/s
R_s	saturated gas solubility, m^3/m^3
SG_g	gas specific density
T	temperature, K
$u(t)$	control variable or output of the PID controller at time t
V	velocity, m/s
V_c	characteristic velocity, m/s
V_S	velocity of the cuttings, m/s
V_M^*	velocity of the liquid–solid mixture in the annulus, m/s
V_{sr}	cuttings settling velocity, m/s
V_G	gas velocity, m/s
V_M	velocity of the gas–liquid–solid mixture, m/s
V_{gr}	gas-phase slip velocity, m/s
x_{L-S}	mass flow fraction of the liquid–solid mixture
x_G	mass flow fraction of the gas phase

Y	gas expansion factor
Z	choke opening

References

1. Sutton, I.S. Summarizing the Deepwater Horizon/Macondo Reports. In Proceedings of the Offshore Technology Conference, Houston, TX, USA, 6–9 May 2013; p. 10.
2. Xie, J.; Zhang, X.; Tang, Y.; Wang, Y.; Shao, Q.; Yu, B. Transient Simulation of the Blowing-Out Process of the Air Pockets in Vertical Wellbore. *Appl. Therm. Eng.* **2014**, *72*, 97–103. [CrossRef]
3. Sleiti, A.K.; Takalkar, G.; El-Naas, M.H.; Hasan, A.R.; Rahman, M.A. Early gas kick detection in vertical wells via transient multiphase flow modelling: A review. *J. Nat. Gas Sci. Eng.* **2020**, *80*, 103391. [CrossRef]
4. Obi, C.E.; Falola, Y.; Manikonda, K.; Hasan, A.R.; Hassan, I.G.; Rahman, M.A. A machine learning approach for gas kick identification. *SPE Drill. Complet.* **2023**, *38*, 663–681. [CrossRef]
5. Chen, X.; He, M.; Xu, M.; Wang, S.; Dai, B. Early gas kick detection-inversion-control integrated system: The significance of applications of managed pressure drilling: A review. *Geoenergy Sci. Eng.* **2023**, *229*, 212134. [CrossRef]
6. Wei, C.; Chen, Y. On improving algorithm efficiency of gas-kick simulations toward automated influx management: A Robertson differential-algebraic-equation problem approach. *SPE Drill. Complet.* **2021**, *36*, 943–966. [CrossRef]
7. Nassab, K.K.; Ting, S.Z.; Buapha, S.; MatNoh, N.; Hemmati, M.N. How to Improve Accuracy of a Kick Tolerance Model by Considering the Effects of Kick Classification, Frictional Losses, Pore Pressure Profile, and Influx Temperature. *SPE Drill. Complet.* **2022**, *37*, 15–25. [CrossRef]
8. Gu, Q.; Fallah, A.; Ambrus, A.; Ma, Z.; Chen, D.; Ashok, P.; van Oort, E. A switching MPD controller for mitigating riser gas unloading events in offshore drilling. *SPE Drill. Complet.* **2020**, *35*, 201–217. [CrossRef]
9. Habib, M.M.; Imtiaz, S.; Khan, F.; Ahmed, S.; Baker, J. Prediction of reservoir-kick effect and its management in the managed-pressure-drilling operation. *SPE Drill. Complet.* **2021**, *36*, 575–602. [CrossRef]
10. Ambrus, A.; Pournazari, P.; Ashok, P.; Shor, R.; van Oort, E. Overcoming Barriers to Adoption of Drilling Automation: Moving Towards Automated Well Manufacturing. In Proceedings of the SPE/IADC Drilling Conference and Exhibition, London, UK, 17–19 March 2015; p. 38.
11. Gravdal, J.E.; Sui, D.; Nagy, A.; Saadallah, N.; Ewald, R. A hybrid test environment for verification of drilling automation systems. In Proceedings of the SPE/IADC Drilling Conference and Exhibition, Virtual, 8–12 March 2021.
12. Lordejani, S.N.; Besselink, B.; Schilders, W.; van de Wouw, N. Model complexity reduction and controller design for managed pressure drilling automation. *J. Process Control.* **2023**, *122*, 69–83. [CrossRef]
13. Jansen, J.D.; van den Steen, L. Active Damping of Self-Excited Torsional Vibrations in Oil Well Drillstrings. *J. Sound Vib.* **1995**, *179*, 647–668. [CrossRef]
14. Runia, D.J.; Dwars, S.; Stulemeijer, I.P.J.M. A Brief History of the Shell "Soft Torque Rotary System" and Some Recent Case Studies. In Proceedings of the SPE/IADC Drilling Conference, Amsterdam, The Netherlands, 5–7 March 2013; p. 10.
15. van Riet, E.J.; Reitsma, D.; Vandecraen, B. Development and Testing of a Fully Automated System to Accurately Control Downhole Pressure During Drilling Operations. In Proceedings of the SPE/IADC Middle East Drilling Technology Conference and Exhibition, Abu Dhabi, United Arab Emirates, 20–23 October 2003; p. 12.
16. Kyllingstad, A.; Nessjøen, P.J. A New Stick-Slip Prevention System. In Proceedings of the SPE/IADC Drilling Conference and Exhibition, Amsterdam, The Netherlands, 17–19 March 2009; p. 14.
17. Florence, F.; Porche, M.; Thomas, R.; Fox, R. Multi-Parameter Autodrilling Capabilities Provide Drilling, Economic Benefits. In Proceedings of the SPE/IADC Drilling Conference and Exhibition, Amsterdam, The Netherlands, 17–19 March 2009; p. 10.
18. Matheus, J.; Naganathan, S. Automation of Directional Drilling—Novel Trajectory Control Algorithms for RSS. In Proceedings of the IADC/SPE Drilling Conference and Exhibition, New Orleans, LA, USA, 2–4 February 2010; p. 10.
19. Godhavn J-m Knudsen, K.A. High Performance and Reliability for MPD Control System Ensured by Extensive Testing. In Proceedings of the IADC/SPE Drilling Conference and Exhibition, New Orleans, LA, USA, 2–4 February 2010; p. 16.
20. Dunlop, J.; Isangulov, R.; Aldred, W.D.; Sanchez, H.A.; Flores, J.L.; Herdoiza, J.A.; Belaskie, J.; Luppens, J.C. Increased Rate of Penetration Through Automation. In Proceedings of the SPE/IADC Drilling Conference and Exhibition, Amsterdam, The Netherlands, 1–3 March 2011; p. 11.
21. Cayeux, E.; Daireaux, B.; Dvergsnes, E. Automation of Mud-Pump Management: Application to Drilling Operations in the North Sea. *SPE Drill. Complet.* **2011**, *26*, 41–51. [CrossRef]
22. Cayeux, E.; Daireaux, B.; Dvergsnes, E. Automation of Drawworks and Topdrive Management To Minimize Swab/Surge and Poor-Downhole-Condition Effect. *SPE Drill. Complet.* **2011**, *26*, 557–568. [CrossRef]
23. Cayeux, E.; Daireaux, B.; Dvergsnes, E.W.; Florence, F. Toward Drilling Automation: On the Necessity of Using Sensors That Relate to Physical Models. *SPE Drill. Complet.* **2014**, *29*, 236–255. [CrossRef]
24. Carlsen, L.A.; Nygaard, G.; Gravdal, J.E.; Nikolaou, M.; Schubert, J. Performing the Dynamic Shut-In Procedure Because of a Kick Incident When Using Automatic Coordinated Control of Pump Rates and Choke-Valve Opening. In Proceedings of the SPE/IADC Managed Pressure Drilling and Underbalanced Operations Conference and Exhibition, Abu Dhabi, United Arab Emirates, 28–29 January 2008; p. 13.

25. Gravdal, J.E.; Nikolaou, M.; Breyholtz, Ø.; Carlsen, L.A. Improved Kick Management During MPD by Real-Time Pore-Pressure Estimation. *SPE Drill. Complet.* **2010**, *25*, 577–584. [CrossRef]
26. Zhou, J.; Stamnes, N.; Aamo, O.M.; Kaasa, G.-O. Switched Control for Pressure Regulation and Kick Attenuation in a Managed Pressure Drilling System. *IEEE Trans. Control. Syst. Technol.* **2011**, *19*, 337–350. [CrossRef]
27. Aarsnes, U.J.F.; Açıkmeşe, B.; Ambrus, A.; Aamo, O.M. Robust Controller Design for Automated Kick Handling in Managed Pressure Drilling. *J. Process Control.* **2016**, *47*, 46–57. [CrossRef]
28. Ma, Z.; Vajargah, A.K.; Ambrus, A.; Ashok, P.; Chen, D.; van Oort, E.; May, R.; Macpherson, J.D.; Becker, G.; Curry, D.A. Multi-Phase Well Control Analysis During Managed Pressure Drilling Operations. In Proceedings of the SPE Annual Technical Conference and Exhibition, Dubai, United Arab Emirates, 26–28 September 2016; p. 21.
29. Ma, Z.; Vajargah, A.K.; Chen, D.; van Oort, E.; May, R.; MacPherson, J.D.; Becker, G.; Curry, D. Gas Kicks in Non-Aqueous Drilling Fluids: A Well Control Challenge. In Proceedings of the IADC/SPE Drilling Conference and Exhibition, Fort Worth, TX, USA, 6–8 March 2018; p. 24.
30. Sule, I.; Imtiaz, S.; Khan, F.; Butt, S. Nonlinear Model Predictive Control of Gas Kick in a Managed Pressure Drilling System. *J. Pet. Sci. Eng.* **2019**, *174*, 1223–1235. [CrossRef]
31. Carlsen, L.A.; Nygaard, G.; Nikolaou, M. Evaluation of Control Methods for Drilling Operations with Unexpected Gas Influx. *J. Process Control.* **2013**, *23*, 306–316. [CrossRef]
32. Hauge, E.; Aamo, O.M.; Godhavn, J. Model-based estimation and control of in/out-flux during drilling. In Proceedings of the American Control Conference (ACC), Montreal, QC, Canada, 27–29 June 2012; pp. 4909–4914.
33. Shishavan, R.A.; Hubbell, C.; Perez, H.; Hedengren, J.; Pixton, D. Combined Rate of Penetration and Pressure Regulation for Drilling Optimization by Use of High-Speed Telemetry. *SPE Drill. Complet.* **2015**, *30*, 17–26. [CrossRef]
34. Olamigoke, O.; James, I. Advances in Well Control: Early Kick Detection and Automated Control Systems. In *Drilling Engineering and Technology-Recent Advances New Perspectives and Applications*; IntechOpen: London, UK, 2022.
35. Erge, O.; Gu, Q.; Chen, D.; van Oort, E. MPD choke control considering the thixotropic gelation behavior of drilling fluids. *J. Pet. Sci. Eng.* **2022**, *208*, 109793. [CrossRef]
36. Li, Q.; Li, Q.; Han, Y. A Numerical Investigation on Kick Control with the Displacement Kill Method during a Well Test in a Deep-Water Gas Reservoir: A Case Study. *Processes* **2024**, *12*, 2090. [CrossRef]
37. Li, Q.; Li, Q.; Wang, F.; Wu, J.; Wang, Y. The Carrying Behavior of Water-Based Fracturing Fluid in Shale Reservoir Fractures and Molecular Dynamics of Sand-Carrying Mechanism. *Processes* **2024**, *12*, 2051. [CrossRef]
38. Shi, H.; Holmes, J.; Diaz, L.R.; Durlofsky, L.J.; Aziz, K. Drift-Flux Parameters for Three-Phase Steady-State Flow in Wellbores. *SPE J.* **2005**, *10*, 130–137. [CrossRef]
39. Shirdel, M.; Sepehrnoori, K. Development of Transient Mechanistic Three-Phase Flow Model for Wellbores. *SPE J.* **2017**, *22*, 374–388. [CrossRef]
40. Zuber, N.; Findlay, J.A. Average Volumetric Concentration in Two-Phase Flow Systems. *J. Heat Transf.* **1965**, *87*, 453–468. [CrossRef]
41. Shi, H.; Holmes, J.A.; Durlofsky, L.J.; Aziz, K.; Diaz, L.R.; Alkaya, B.; Oddie, G. Drift-Flux Modeling of Two-Phase Flow in Wellbores. *SPE J.* **2005**, *10*, 24–33. [CrossRef]
42. Livescu, S.; Durlofsky, L.J.J.; Aziz, K. A Semianalytical Thermal Multiphase Wellbore-Flow Model for Use in Reservoir Simulation. *SPE J.* **2010**, *15*, 794–804. [CrossRef]
43. Guet, S.; Ooms, G. Fluid Mechanical Aspects of the Gas-Lift Technique. *Annu. Rev. Fluid Mech.* **2005**, *38*, 225–249. [CrossRef]
44. Hasan, A.R.; Kabir, C.S.; Sayarpour, M. A Basic Approach to Wellbore Two-Phase Flow Modeling. In Proceedings of the SPE Annual Technical Conference and Exhibition, Anaheim, CA, USA, 11–14 November 2007; p. 9.
45. Pan, L.; Webb, S.W.; Oldenburg, C.M. Analytical Solution for Two-Phase Flow in a Wellbore using the Drift-Flux Model. *Adv. Water Resour.* **2011**, *34*, 1656–1665. [CrossRef]
46. Standing, M.B. A pressure-volume-temperature correlation for mixtures of California oils and gases. In Proceedings of the Drilling and Production Practice, New York, NY, USA, 1 January 1947.
47. Yoshinaga, T.; Sato, Y. Performance of an Air-Lift Pump for Conveying Coarse Particles. *Int. J. Multiph. Flow* **1996**, *22*, 223–238. [CrossRef]